# Formation and migration of charged native point defects in $MgH_2$: First-principles calculations

Min Sik Park, Anderson Janotti, and Chris G. Van de Walle
*Materials Department, University of California, Santa Barbara, California 93106-5050, USA*
(Received 19 January 2009; revised manuscript received 30 April 2009; published 4 August 2009)

Using first-principles calculations we have investigated the possible native point defects in bulk $MgH_2$. Due to the interest in this material for hydrogen storage, we have paid particular attention to hydrogen-related defects that are likely to be involved in the absorption and release kinetics of hydrogen. We have considered neutral and charged defects and calculated formation energies as a function of Fermi-level position and hydrogen chemical potential. In the absence of impurities, we find that under extreme H-poor conditions the lowest-energy defects are positively and negatively charged hydrogen vacancies ($V_H^+$ and $V_H^-$). Under extreme H-rich conditions, the lowest-energy defects are $V_H^+$, negatively charged hydrogen interstitials ($H_i^-$), and negatively charged Mg vacancies $V_{Mg}^{2-}$. The defects are characterized by unusually large local structural rearrangements. The hydrogen-related defects are also highly mobile, with a lowest migration barrier of less than 0.10 eV for $H_i^-$ and $H_{2i}$, and a highest barrier of 0.63 eV for $V_H^-$. By combining the calculated formation energies with migration barriers, we find that the lowest activation energy for self-diffusion is about 1.48 eV under H-poor conditions. The consequences of these results for the hydrogenation and dehydrogenation kinetics are discussed.

DOI: 10.1103/PhysRevB.80.064102 PACS number(s): 66.30.H−, 61.72.Bb, 71.55.Ht, 84.60.Ve

## I. INTRODUCTION

Hydrogen storage materials have been receiving a great deal of attention because of their importance to future systems in which hydrogen serves as an energy carrier at the core of a carbon-neutral system of energy production and use. In particular, hydrogen storage materials for mobile applications can contribute to overcoming problems related to fossil fuel dependence and climate change. The search is on to find materials that can efficiently store hydrogen and that also display appropriate kinetics for absorption and release of hydrogen. Storing hydrogen in solid-state materials stands out by its safety and can also feature high volumetric and gravimetric densities.[1–3]

$MgH_2$ has great potential as a hydrogen storage material due to its high capacity of 7.6 wt %.[1,3] However, its slow hydrogenation and dehydrogenation kinetics, and the required high temperature of ~300 °C for decomposition are major obstacles for mobile applications.[3,4] Understanding the microscopic mechanisms behind the hydrogenation and dehydrogenation processes is key to engineering solutions—e.g., in the form of a catalytic process—to speed the kinetics and to lowering the decomposition temperature. Diffusion in solids is mediated by point defects; the microscopic mechanisms behind the hydrogenation and dehydrogenation of $MgH_2$ are therefore related to the formation and diffusivity of point defects in bulk $MgH_2$. From this perspective, it is essential to understand the defect physics as well as the migration mechanisms and barriers in $MgH_2$.

Several experimental and theoretical investigations of defects in $MgH_2$ have been published.[5–12] However, most of them have concentrated on macroscopic analysis of thermodynamic measurements, surface defects, or exclusively neutral point defects in bulk $MgH_2$. As noted in Ref. 12, $MgH_2$ is a wide band-gap material in which point defects are likely to exist in charge states other than neutral. The presence of charged defects is not incompatible with the behavior of $MgH_2$ as an insulator: positively and negatively charged defects occur in equal concentrations and compensate each other. No free carriers are present and the Fermi-level position, determined by the charge neutrality condition, is far from the conduction- and valence-band edges, as expected for an insulator. In the absence of impurities the Fermi-level position will be determined by those native point defects that have the lowest formation energy and opposite charges.

We have performed first-principles calculations of all relevant point defects in bulk $MgH_2$, in all possible charge states. Both H-rich and H-poor conditions are considered.[13] In addition to calculating formation energies, we have explored the possible migration paths and calculated the lowest migration barriers for the relevant defects. By combining formation energies and energy barriers we have derived the activation energies for different self-diffusion mechanisms. Similar to sodium alanate ($NaAlH_4$), another candidate for hydrogen storage, we find that the relevant defects are most stable in non-neutral charge states.[14,15] We also find that the defects are characterized by large local atomic rearrangements. The calculated migration barriers are all relatively low, rendering the defects mobile even below room temperature. Consequences for dehydrogenation and hydrogenation processes will be discussed.

## II. METHODOLOGY

The calculations are based on density-functional theory (DFT) within the generalized gradient approximation (GGA) (Ref. 16) and the projector augmented wave method as implemented in the VASP code.[17,18] The defects were simulated using 72-atom supercells, and the Brillouin-zone integrations implemented by summations over a mesh of $2\times2\times2$ special $k$ points, with an energy cutoff of 250 eV for the plane-wave basis set.

$MgH_2$ crystallizes in the rutile structure shown in Fig. 1. The calculated lattice parameters $c=2.99$ Å, $c/a=0.67$, and

 

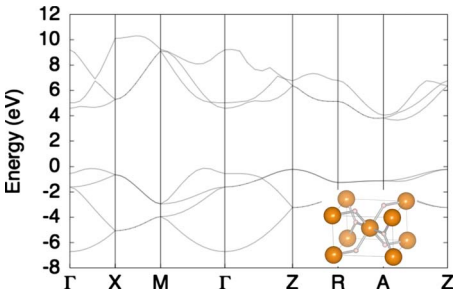


FIG. 1. (Color online) Calculated band structure of $MgH_2$. The inset shows the crystal structure of rutile $MgH_2$; large spheres are Mg, small spheres are H atoms.

$u=0.304$ are in good agreement with experimental values of 3.01 Å, 0.67, and 0.304.[19] The calculated formation enthalpy of bulk $MgH_2$ relative to bulk Mg and the isolated $H_2$ molecule is $\Delta H_f(MgH_2)=-0.66$ eV, in good agreement with the experimental value of −0.68 eV.[20] The band structure of $MgH_2$ is shown in Fig. 1. The calculated indirect band gap of $MgH_2$ of 3.8 eV is smaller than the reported experimental values that range from 5.16 to 6.05 eV.[21] This underestimation is typical in DFT-GGA calculations. We find that the valence-band maximum (VBM) is derived mainly from H 1*s* states and the conduction-band minimum (CBM) mainly from Mg 3*s* states.

In the dilute limit, the concentration of defects in the solid is determined by their formation energy

$$c = N_{\text{sites}} \exp(-E^f/kT), \tag{1}$$

where $E^f$ is the formation energy, $N_{\text{sites}}$ is the number of sites on which the defect can be incorporated, $k$ is the Boltzmann constant, and $T$ is the temperature. The formation energy $E^f$ of a defect $X$ in charge state $q$ is given by[13]

$$E^f(X^q) = E_{\text{tot}}(X^q) - E_{\text{tot}}(\text{bulk}) - \sum_i n_i(\mu_i + E_{ref,i}) + qE_F, \tag{2}$$

where $E_{\text{tot}}(X^q)$ and $E_{\text{tot}}(\text{bulk})$ are the total energies of a supercell containing the defect in charge state $q$ and of the perfect crystal in the same supercell, respectively. $\mu_i$ is the chemical potential of species $i$ and $n_i$ is the number of atoms of species $i$ added to ($n_i>0$) or removed from ($n_i<0$) the supercell to form the defect. The chemical potentials $\mu_H$ and $\mu_{Mg}$ are referenced to the energy per atom of an $H_2$ molecule [$E_{ref,H}=1/2E_{\text{tot}}(H_2)$] and to the energy per atom of bulk Mg [$E_{ref,Mg}=E_{\text{tot}}(Mg)$], respectively, and are subject to boundaries given by the stability of $MgH_2$[$\mu_{Mg}+2\mu_H=\Delta H_f(MgH_2)$], as well as $\mu_{Mg}\leq 0$ and $\mu_H\leq 0$. $E_F$, finally, is the energy of the electron reservoir or Fermi level, which is referenced to the VBM. The VBM in the defect cell and the perfect-crystal cell were aligned by taking the averaged electrostatic potential far from the defect as described in Ref. 13.

The calculations of migration barriers were performed by taking several points along a line connecting the initial and final positions, and allowing the migrating species to fully relax in a plane perpendicular to the migration direction. The migration barrier is then defined as the energy difference between the initial and the saddle-point configurations.

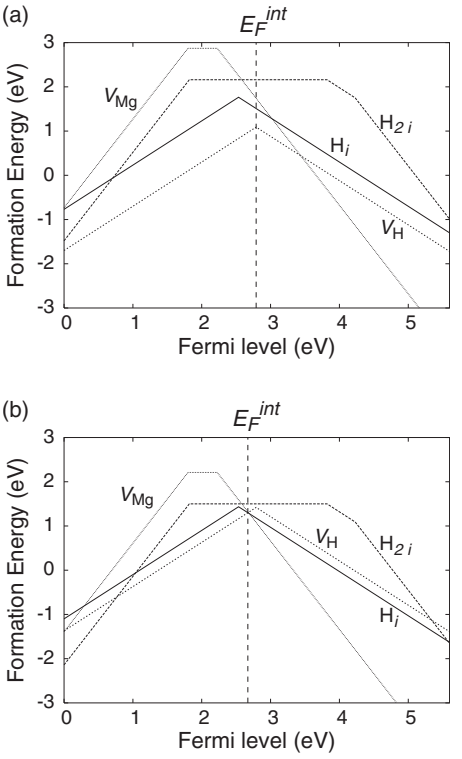


FIG. 2. Formation energies as a function of Fermi level in bulk $MgH_2$ for native point defects, $H_i$, $H_{2i}$, $V_H$, and $V_{Mg}$, in various charge states under (a) H-poor and (b) H-rich conditions.

## III. RESULTS

### A. Formation energy and atomic structure

The calculated formation energies as a function of the Fermi-level $E_F$ for the most relevant defects are shown in Fig. 2. Under extreme H-poor conditions [$\mu_{Mg}=0$ and $\mu_H=1/2\Delta H_f(MgH_2)$] shown in Fig. 2(a), the lowest-energy defects in $MgH_2$ are $V_H$ and $V_{Mg}$. If no other defects or impurities are present, charge neutrality would pin the Fermi level at 2.79 eV, where $V_H^+$ and $V_H^-$ have equal formation energies $E^f=1.10$ eV.

Under extreme H-rich conditions [$\mu_H=0$ and $\mu_{Mg}=\Delta H_f(MgH_2)$] our results indicate that the relevant defects are $V_H^+$, $H_i^-$, and $V_{Mg}^{2-}$. These defects happen to have the same formation energy $E^f=1.30$ eV at the Fermi-level value $E_F^{\text{int}}=2.67$ eV where their formation energies intersect. Assuming that $V_H^+$, $H_i^-$, and $V_{Mg}^{2-}$ are the dominant defects and in the absence of free carriers, the Fermi-level position is determined by the charge neutrality condition which imposes that the total amount of positive charge (equal to the concentration of $V_H^+$) is equal to the total amount of negative charge (the sum of the concentration of $H_i^-$ plus twice the concentration of $V_{Mg}^{2-}$). The resulting Fermi level is then slightly lower than the value 2.67 eV where the formation energies intersect. An explicit solution of the charge neutrality equations shows that, at 600 K, the Fermi level is positioned at 2.66 eV, i.e., within 0.01 eV of the point where the formation energies intersect. The formation energy of $H_i^+$ is slightly higher (by 0.27 eV) than that of $V_H^+$, and the formation en-

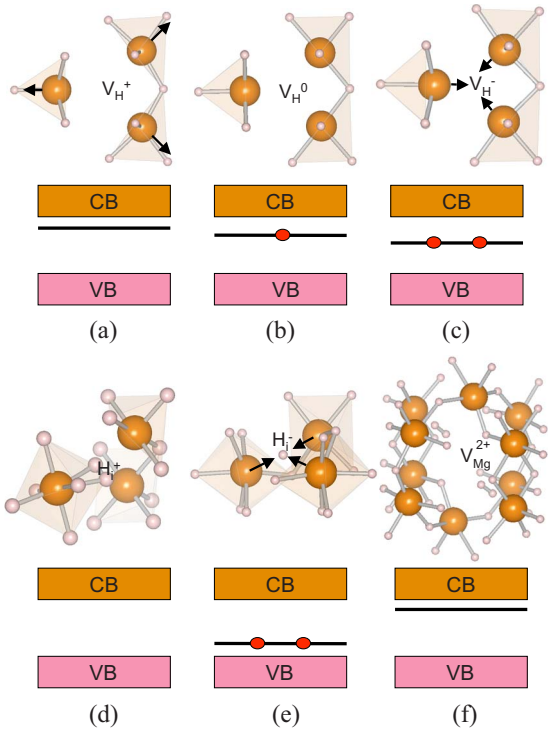


FIG. 3. (Color online) Structural rearrangements around charged native point defects in $MgH_2$ and schematic diagrams of single-particle states and electron occupations. (a) $V_H^+$, (b) $V_H^0$, (c) $V_H^-$, (d) $H_i^+$, (e) $H_i^-$, and (f) $V_{Mg}^{2+}$.

ergy of $V_H^-$ is slightly higher (by 0.24 eV) than that of $H_i^-$, as shown in Fig. 2(b).

The local atomic relaxations around $V_H$ are shown in Figs. 3(a)–3(c). The electronic structure can be understood as follows. The removal of a hydrogen atom results in a single-particle state located in the band gap occupied by one electron [Fig. 3(b)]. This state is a symmetric combination of the 3*s* states of the three nearest-neighbor Mg atoms. In this neutral charge state the atomic relaxations are very small (0.01 Å change from bulk positions). Upon removal of the electron ($V_H^+$) the three nearest-neighbor Mg atoms relax outward by ~14% of the Mg-H equilibrium distance [Fig. 3(a)]. In the absence of this electron the system does not gain any electronic energy by having the three nearest-neighbor Mg atoms nearby and they relax outward to strengthen their bonding with the rest of the lattice. The empty single-particle state moves up to near the CBM [Fig. 3(a)]. On the other hand, upon addition of an electron ($V_H^-$) the three nearest-neighbor Mg atoms relax inward in order to strengthen their bonding with each other. Two of the Mg atoms move by 8% of the equilibrium Mg-H distance, the other by 15%. The doubly occupied single-particle state is now located near the middle of the gap [Fig. 3(c)]. Note that $V_H^0$ itself is unstable (and hence not included in Fig. 2); this is characteristic of a negative-*U* center in which the formation energy of the neutral charge state (1.96 eV under H-poor conditions) is higher than that of either the positive or negative charge for any value of the Fermi level in the band gap. This pattern of relaxation versus charge states has also been observed for oxygen vacancies in wurtzite ZnO and rutile $SnO_2$.[22,23]

Since $V_H$ can assume the negative and positive charge states, it is of interest to investigate complexes formed by two neighboring $V_H$, considering that $V_H^+$ and $V_H^-$ can bind to form a neutral complex. We find that the complex $2V_H^0$ is most stable when the distance between the vacancies is the shortest, i.e., when the vacancies lie in the same basal plane, aligned along the [110] direction, and thus have two Mg atoms as common nearest neighbors. The relaxations around the vacancies are small, with the two neighboring Mg atoms in the basal plane moving away from the vacancies by 0.03 Å. The formation energy for this complex is 1.78 eV under H-poor conditions and the binding energy with respect to two isolated vacancies is 0.42 eV. Given the fairly high formation energy, we expect $2V_H^0$ complexes to be present only in low concentrations, such that they will not play a role in the dehydrogenation process.

The different charge states of the interstitial, $H_i^+$ and $H_i^-$, give rise to very different local lattice rearrangements. In the case of $H_i^+$, the extra H forms an $H_2$ molecule with the nearest H host atom, as shown in Fig. 3(d). This is in agreement with what is observed in semiconductors, where $H_i^+$ forms a strong bond with the anion.[24] The calculated H-H bond length is 0.77 Å, slightly larger than the 0.75 Å bond length calculated in a free $H_2$ molecule. As a result of this large local lattice rearrangement we find that $H_i^+$ does not induce states in the band gap. This is in contrast to the "ideal" interstitial H configuration—where H is placed at the tetrahedral interstitial site—which has an associated single-particle state at ~1 eV above the VBM.

In the case of $H_i^-$, the extra H is stable near a tetrahedral interstitial site. The four nearest-neighbor H host atoms relax outwards from the tetrahedral site by as much as 0.52 Å, whereas the four Mg atoms relax inward by 0.21 Å, as shown in Fig. 3(e). This can be explained by the Coulomb repulsion between $H_i^-$ and the H anions, and the Coulomb attraction between $H_i^-$ and the Mg cations in the $MgH_2$ lattice. We find that $H_i^-$ induces a doubly occupied single-particle state located ~1 eV above the VBM [Fig. 3(e)]. Similarly to the hydrogen vacancy, we find that the neutral interstitial $H_i^0$ is unstable for all Fermi-level positions in the band gap (the formation energy of $H_i^0$ is 2.87 eV under H-poor conditions), i.e., it is a negative-*U* center with the (+/−) transition level (Fermi-level position where the stability changes from $H_i^+$ to $H_i^-$) at 2.54 eV above the VBM.

We have also considered an interstitial $H_2$ molecule, i.e., the addition of two H atoms. Under H-rich conditions, the formation energy of neutral interstitial $H_2$ is $E^f = 1.45$ eV. The center of mass of the interstitial $H_2$ is located near the octahedral interstitial site, with the H-H bond in the (001) plane (close to the [100] direction) and an H-H distance of 0.76 Å. For $E_F \leq 1.80$ eV, $H_{2i}^{2+}$ has the lowest formation energy. In this charge state, the added H atoms form *two* $H_2$ molecules by combining with two H host atoms as in the case of $H_i^+$. For $3.87 \leq E_F \leq 4.23$ eV, $H_{2i}^-$ is stable, in which the interstitial $H_2$ molecule has its center of mass near the octahedral site. For $E_F \geq 4.23$ eV, $H_{2i}^{2-}$ is stable, with the center of mass near the tetrahedral site.

Turning now to Mg-site defects, we investigated interstitial Mg, considering five charge states from −2 to +2. Among the charge states, the lowest formation energy was found for

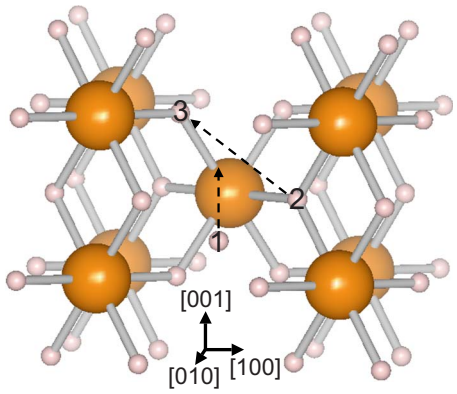


FIG. 4. (Color online) Ball-and-stick model of $MgH_2$; specific hydrogen atoms are labeled to aid in describing diffusion paths of $H_i^+$, $H_i^-$, $V_H^+$, and $V_H^-$. Site 1 is the location of a hydrogen interstitial in the negative charge state.

$Mg_i^{2+}$ (2.11 eV at $E_F^{int}=2.79$ eV under H-poor conditions). This is considerably higher than the formation energy of the other defects and for that reason not included in Fig. 2. The $Mg_i^{2+}$ is stable at the octahedral site and it forms a $MgH_6$ octahedron with six nearest-neighbor H host atoms.

For the Mg vacancy, $V_{Mg}$, we find a very unusual behavior. Cation vacancies in ionic materials normally act exclusively as acceptors. However, we find that $V_{Mg}$ is amphoteric, acting either as a donor or an acceptor depending on the position of the Fermi level. This behavior is a result of very large local lattice rearrangements that strongly depend on the charge state of the defect. For $E_F \leq 1.80$ eV, $V_{Mg}^{2+}$ has the lowest energy. In this case, four of the six nearest-neighbor H atoms strongly relax to form two $H_2$ molecules with interatomic distances of 0.77 Å [Fig. 3(f)]. For $1.80 \leq E_F \leq 2.23$ eV, the Mg vacancy is stable in the neutral charge state $V_{Mg}^0$, in which one $H_2$ molecule with an interatomic distance of 0.77 Å is formed near the vacancy center. For $E_F \geq 2.23$ eV, $V_{Mg}^{2-}$ has the lowest energy with six nearest-neighbor H atoms relaxing outwards.

### B. Diffusion

In addition to the formation energies, we have also investigated the migration of the hydrogen-related defects in $MgH_2$. We have explored possible migration paths and calculated energy barriers for $H_i^+$, $H_i^-$, $V_H^+$, $V_H^-$, and $V_{Mg}^{2-}$. Starting with the Mg vacancy, we find a migration barrier of 0.74 eV for a neighboring Mg atom to move into the vacancy. This motion would be relevant for transport of Mg but as we shall see transport of hydrogen can proceed with lower activation energies. In the case of $H_i^+$, we find the lowest migration barrier for path $2 \rightarrow 3$ in Fig. 4 with a barrier of 0.12 eV. Along this path, $H_i^+$ forms an $H_2$ molecule with the H atom on lattice site 2 in the initial configuration and lattice site 3 in the final configuration. This path can account for displacement along any of the crystallographic axes and therefore the diffusion of $H_i^+$ will be isotropic. In contrast, the migration of $H_i^-$ is anisotropic with energy barriers of 0.02 and 0.33 eV along [001] (path 1 in Fig. 4) and [110] directions, respectively. Because of their low migration barriers, these defects will be mobile even below room temperature. The anisotropy of $H_i^-$ would only be revealed at very low temperatures (where the concentration of hydrogen-related defects will be very low).

TABLE I. Calculated formation energies $E^f$, migration barriers $E_b$, and diffusion activation energies $Q=E^f+E_b$ for hydrogen-related native point defects in $MgH_2$. Values are given for hydrogen-poor and hydrogen-rich conditions, as defined in the text. When the migration path is anisotropic, two values are given for $E_b$ and $Q$, the first corresponding to diffusion along [001], the second along [110].

| Conditions | Defect | $E^f$ (eV) | $E_b$ (eV) | $Q$ (eV) |
|---|---|---|---|---|
| H poor | $V_H^+$ | 1.10 | 0.38 | 1.48 |
| | $V_H^-$ | 1.10 | 0.63 | 1.73 |
| | $H_i^+$ | 2.01 | 0.12 | 2.13 |
| | $H_i^-$ | 1.51 | 0.02/0.33 | 1.53/1.84 |
| | $H_{2i}^0$ | 2.13 | 0.05/0.53 | 2.18/2.66 |
| H rich | $V_H^+$ | 1.30 | 0.38 | 1.68 |
| | $V_H^-$ | 1.54 | 0.63 | 2.17 |
| | $H_i^+$ | 1.57 | 0.12 | 1.69 |
| | $H_i^-$ | 1.30 | 0.02/0.33 | 1.32/1.63 |
| | $H_{2i}^0$ | 1.47 | 0.05/0.53 | 1.52/2.00 |

For both $V_H^+$ and $V_H^-$, we find that the migration is isotropic with the lowest migration barriers of 0.38 for $V_H^+$ and 0.63 eV for $V_H^-$ for the path $2 \rightarrow 3$ in Fig. 4. Finally, we have also calculated the migration path of $H_{2i}^0$. Along the [001] direction, we find a very low barrier of only 0.05 eV; along the [110] direction, the barrier is 0.53 eV.

Our calculations allow us to extract activation energies for self-diffusion, defined as the sum of the formation energy and the migration barrier ($Q=E^f+E_b$). A summary of our results is presented in Table I for both hydrogen-rich and hydrogen-poor conditions.

A comparison between our calculated diffusion activation energies with experimental numbers may shed light on the dominant diffusion mechanism under specific experimental conditions. Under H-poor conditions, we find that $V_H^+$ and $V_H^-$ are the dominant defects (see Fig. 2). In order to maintain local charge neutrality, both positively and negatively charged vacancies would need to be present. The diffusion activation energy of $V_H^+$, $Q=1.48$ eV, falls at the center of the experimentally reported range. The activation energy of $V_H^-$ is higher (1.73 eV) and this could, in principle, form a bottleneck. However, if the oppositely charged vacancies remain in close proximity during the diffusion process they will be able to exchange electrons, allowing the more mobile $V_H^+$ to drive the process.

The lowest activation energy $Q$ under H-rich conditions is close to that under H-poor conditions but the diffusion mechanism is different. The defect with the lowest activation energy is $H_i^-$ ($Q=1.32$ eV for diffusion along [001] and 1.63 eV for diffusion along [110]) but the interstitial molecule $H_{2i}$ has an activation energy of 1.52 eV along the [001] direction and automatically satisfies charge neutrality.

A variety of experimental values have been reported for activation energies for hydrogen desorption from $MgH_2$, ranging from 1.24 to 1.66 eV (Ref. 6 and references therein). Assuming that desorption experiments correspond to hydrogen-poor conditions, we find good agreement with our numbers for hydrogen vacancies.

It is also interesting to compare our values with the results of nuclear-magnetic-resonance (NMR) experiments[7,25] in which the rate of H hopping is determined from spin-relaxation times and line narrowing. In these experiments the $MgH_2$ sample is sealed into a glass tube under 0.9 atm $N_2$; it is not immediately clear what the corresponding value of the hydrogen chemical potential would be. In any event, as noted above the activation energy for self-diffusion under H-rich conditions is not significantly different from that under H-poor conditions. The NMR measurements have resulted in activation energies of 1.45 eV (Ref. 7) and 1.72 eV (Ref. 25). Our calculated values are in broad agreement with these results but the activation energies for the different processes are too similar to allow for a microscopic identification of the diffusion mechanism.

## IV. SUMMARY

In summary, we have determined the relevant defect species and their migration barriers in bulk $MgH_2$ on the basis of first-principles calculations. Unusually large local structural rearrangements were found. Calculated activation energies for hydrogen self-diffusion fall within the range of activation energies reported for hydrogen desorption. Hydrogen diffusion must therefore be an important mechanism in desorption.

## ACKNOWLEDGMENTS

We thank M. S. Conradi for useful discussions and for sharing unpublished data. This work was supported by the U.S. Department of Energy (Award No. DE-FG02-07ER46434) and by the University of California Energy Institute. It made use of the CNSI Computing Facility under NSF Grant No. CHE-0321368 and the TeraGrid computing resources under Grant No. TG-DMR070072N.

[1] J. A. Ritter, A. D. Ebner, J. Wang, and R. Zidan, Mater. Today **6**, 18 (2003).
[2] G. W. Crabtree, M. S. Dresselhaus, and M. V. Buchanan, Phys. Today **57** (12), 39 (2004).
[3] L. Schlapbach and A. Züttel, Nature (London) **414**, 353 (2001).
[4] B. Bogdanovic, K. Bohmhammel, B. Christ, A. Reiser, K. Schlichte, R. Vehlen, and U. Wolf, J. Alloys Compd. **282**, 84 (1999).
[5] J. Huot, G. Liang, S. Boily, A. Van Veste, and R. Schulz, J. Alloys Compd. **293-295**, 495 (1999).
[6] J. F. Fernández and C. R. Sánchez, J. Alloys Compd. **340**, 189 (2002).
[7] M. S. Conradi, M. P. Mendenhall, T. M. Ivancic, E. A. Carl, C. D. Browning, P. H. L. Notten, W. P. Kalisvaart, P. C. M. M. Magusin, R. C. Bowman, Jr., S.-J. Hwang, and N. L. Adolphi, J. Alloys Compd. **446-447**, 499 (2007).
[8] J. Grbović Novaković, Lj. Matović, M. Drvendzija, N. Novaković, D. Rajnović, M. Siljegović, Z. Kačarević Popović, S. Milovanović, and N. Ivanović, Int. J. Hydrogen Energy **33**, 1876 (2008).
[9] A. J. Du, S. C. Smith, X. D. Yao, and G. Q. Lu, Surf. Sci. **600**, 1854 (2006).
[10] A. J. Du, S. C. Smith, and G. Q. Lu, J. Phys. Chem. C **111**, 8360 (2007).
[11] T. Kelkar, S. Pal, and D. G. Kanhere, ChemPhysChem **9**, 928 (2008).
[12] S. Hao and D. S. Sholl, Appl. Phys. Lett. **93**, 251901 (2008).
[13] C. G. Van de Walle and J. Neugebauer, J. Appl. Phys. **95**, 3851 (2004).
[14] A. Peles and C. G. Van de Walle, Phys. Rev. B **76**, 214101 (2007).
[15] C. G. Van de Walle, A. Peles, A. Janotti, and G. B. Wilson-Short, Physica B **404**, 793 (2009).
[16] J. P. Perdew, J. A. Chevary, S. H. Vosko, K. A. Jackson, M. R. Pederson, D. J. Singh, and C. Fiolhais, Phys. Rev. B **46**, 6671 (1992).
[17] G. Kresse and J. Furthmüller, Phys. Rev. B **54**, 11169 (1996).
[18] G. Kresse and D. Joubert, Phys. Rev. B **59**, 1758 (1999).
[19] M. Bortz, B. Bertheville, G. Böttger, and K. Yvon, J. Alloys Compd. **287**, L4 (1999).
[20] *CRC Handbook of Chemistry and Physics*, 83rd ed., edited by D. R. Lide (CRC, New York, 2002).
[21] J. Isidorsson, I. A. M. E. Giebels, H. Arwin, and R. Griessen, Phys. Rev. B **68**, 115112 (2003), and references therein.
[22] A. Janotti and C. G. Van de Walle, Appl. Phys. Lett. **87**, 122102 (2005).
[23] A. K. Singh, A. Janotti, M. Scheffler, and C. G. Van de Walle, Phys. Rev. Lett. **101**, 055502 (2008).
[24] C. G. Van de Walle and J. Neugebauer, Nature (London) **423**, 626 (2003).
[25] R. L. Corey, T. M. Ivancic, D. T. Shane, E. A. Carl, R. C. Bowman, Jr., J. M. Bellosta von Colbe, M. Dornheim, R. Bormann, J. Huot, R. Zidan, A. C. Stowe, and M. S. Conradi, J. Phys. Chem. C **112**, 19784 (2008).